

# Influence of human breathing modes on airborne cross infection risk

JM Villafruela <sup>a,\*</sup>, I Olmedo <sup>b</sup>, JF San José <sup>a</sup>

<sup>a</sup>*Department of Energy and Fluid Mechanics, University of Valladolid, 47011 Valladolid, Spain.*

<sup>b</sup>*Department of Chemical Physics and Applied Thermodynamics, Cordoba University, 14014 Córdoba, Spain.*

*\*Corresponding Author.*

*Tel: +34 983 184 408*

*Fax: +34 983 423 363*

*Email: manolo@eii.uva.es*

## **Abstract**

CFD simulation is an accurate and reliable method to predict the risk of airborne cross-infection in a room. This paper focuses on the validation of a 3-D transient CFD model used to predict personal exposure to airborne pathogens and infection risk in a displacement ventilated room. The model provides spatial and temporal solutions of the airflow pattern in the room (temperature, velocity and turbulence), as well as contaminant concentration in a room where two thermal manikins simulate two standing people, one of whom exhales a tracer gas N<sub>2</sub>O simulating airborne contaminants. Numerical results are validated with experimental data and the model shows a high accuracy when predicting the transient cases studied. Once the model is validated, the CFD model is used to simulate different airborne cross-infection risk scenarios. Four different combinations of the manikins' breathing modes and four different separation distances between the two manikins are studied. The results show that exhaling through the nose or mouth disperses exhaled contaminants in a completely different way and also means that exhaled contaminants are received differently. For short separation distances between breathing sources the interaction between breaths is a key factor in the airborne cross-infection for all the breathing mode combinations studied. However, for long distances the general airflow conditions in the room prove to be more important.

## **1. Introduction**

CFD has been used to obtain spatial and temporal solutions of the characteristics of indoor airflow patterns over the last 40 years. The first numerical results of CFD in indoor environments were based on predicting velocity fields and air distribution in rooms [1-4]. Later, analysis of different air diffusers and airflow patterns generated in ventilated spaces also became an important issue in CFD studies [5-9].

As the capacity of computers and numerical models grew, CFD simulations of indoor environments became more complex. Airflow patterns, temperature fields and the contaminant distribution of occupied rooms using different heating, cooling and ventilation systems were numerically analyzed for many years. These simulations included thermal loads, such as people and airborne contaminants (VOCs, particles or airborne pathogens) [10-18].

People were first considered as thermal loads, and later a person's breathing was also taken into account as a source of contaminants. A person infected by any virus or bacteria, such as measles, flu or tuberculosis, may exhale small droplet nuclei that are basically carried by the airflow [19,20]. These particles may be rebreathed by other people in the room causing a risk of infection. Realistic cases of airborne cross-infection situations have been studied by means of CFD using, in many cases, experimental measurements to validate models and their results. Particularly after the SARS outbreak in 2003, the need to obtain fast and reliable answers to the origin and mechanisms of airborne infection transmission linked to CFD began to take on a key role in this research field [21-25]. In recent years, CFD simulations have been used to analyze and understand the diffusion of exhaled contaminants in different indoor environments, such as operating theatres and isolation rooms [26-31], hospital wards [32,33] offices [34,35] or rail and aircraft cabins [36-38]. All this research evidences that CFD is an important tool vis-à-vis obtaining answers to the complex airborne infection route. Particular effort has been made to study the human breathing processes involved in the airborne transmission routes of diseases, such as coughing [39-41], sneezing [42,43] or breathing exhalation and inhalation [44-49].

However, transient analysis of breathing processes and the dispersion of exhaled contaminants remains limited. Human respiration processes, such as breathing, are transient and change their characteristics over a short period of time. This makes it difficult for experimental techniques to take measurements at the same pace as breathing conditions change [40,50,51]. Most CFD simulations consider the breathing process as steady, and assume a constant exhalation velocity value. This simplifies the problem studied. However, the dynamic characteristics of the breathing process are not studied and, therefore, accuracy when predicting the dispersion of exhaled contaminants may be reduced.

This paper proposes a transient study of the dispersion of exhaled contaminants and of the interaction between the respiration flows of two people in a displacement-ventilated room. In order to achieve this objective, a CFD model reproduces with a high degree of accuracy the experimental tests carried out in a full-scale test room with two breathing thermal manikins [52]. The exhalation of the source manikin (SM) contains a tracer gas simulating fine droplets ( $<5\mu\text{m}$  in diameter) which may contain biological contaminants. This work focuses only on the spread of these small exhaled droplets that follow the air stream because of their small size [19]. The second manikin, considered the target (TM), is placed in front of the SM and is susceptible to inhaling the contaminants exhaled by the source and so become infected by certain pathogens. CFD simulations allow a realistic analysis of the dispersion of exhaled contaminants over time and a study of how they influence the TM's microenvironment. The amount of contaminants inhaled by the TM at different instants is also studied. The target manikin's risk of airborne cross-infection is studied considering different separation distances between the manikins (0.35 m, 0.50 m, 0.80 m and 1.10 m). The experimental results [52] are used to validate the numerical simulations.

The second objective of this paper is to analyze the same risk situation between the two manikins but modifying their breathing modes in order to predict how this parameter impacts on the dispersion of exhaled contaminants and therefore on personal exposure caused to the TM. Four combinations of exhalation modes are studied (see Table 1). The two manikins always inhale through the nose.

Table 1: Exhalation modes for the two manikins. The manikins always inhale through the nose.

Test	Target Manikin (TM)	Source Manikin (SM)
MM	Mouth	Mouth
NM	Nose	Mouth
MN	Mouth	Nose
NN	Nose	Nose

Each test is studied for four different separation distances between the two manikins (0.35 m, 0.50 m, 0.80 m and 1.10 m), thereby obtaining 16 different simulated situations.

## 2. Experimental method

The numerical results obtained with CFD are validated with results of experimental tests carried out in a test room at Aalborg University, the room measuring 4.1 m in length, 3.2 m in width and 2.7 m in height (Fig. 1). In the middle of the left-hand wall a semi-cylindrical displacement diffuser is mounted. This measures 0.6 m in height and has a 0.1 m radius, and provides a cold air supply at 16°C with an air exchange rate of 5.6 h. Two rectangular exhaust openings measuring 0.3 m × 0.1 m each are placed in the two upper corners of the same wall as the diffuser. A radiator measuring 0.55 m × 0.40 m × 0.05 m is also placed in the middle plane of the test room. The heat load of the radiator is maintained at 300 W.

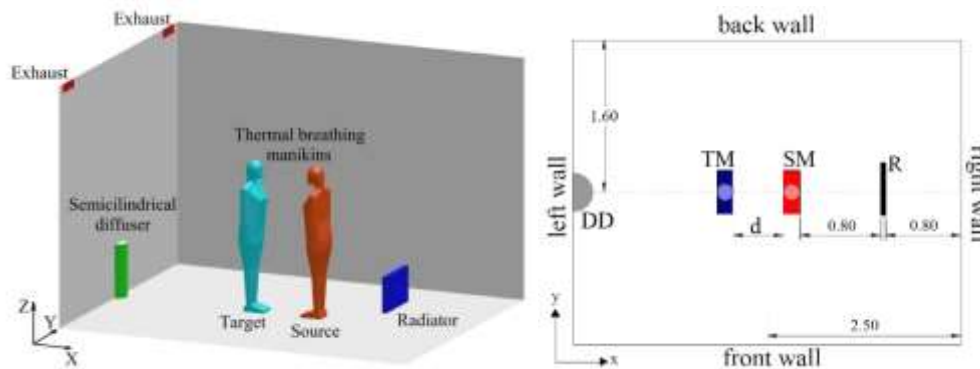


Fig. 1 Setup of the test room with the two thermal breathing manikins (SM: source manikin, and TM: target manikin) separated by a distance  $d=0.50$  m, the semi-cylindrical displacement diffuser (DD) and the radiator (R). All measurements are in meters

Two thermal breathing manikins are placed in the room facing each other (Fig. 1). The manikins are placed along the central plane of the room. The source manikin (SM) is considered to be an infected person and exhales contaminants simulated using a tracer gas,  $N_2O$ . This contaminant source provokes a risk situation of contagion to the susceptible person located in the same room. The target manikin (TM) simulates the susceptible person.

The SM was always 0.80 m from the radiator. Four different distances ( $d$ ) between the manikins (0.35 m, 0.5 m, 0.8 m and 1.1 m) are used to study its influence on the cross-infection risk. The manikins are 1.68 m tall, average-size women. Each manikin is responsible for 94 W of heat load. The breathing functions of the manikins were performed by artificial lungs, presenting a sinusoidal airflow shape.

In the experiments, both manikins exhale through the mouth and inhale through the nose. The nostrils have an angle with the horizontal plane of about  $45^\circ$  and an angle with the intervening angle of  $30^\circ$  between the vertical planes. The mouths have a  $123 \text{ mm}^2$  opening and a semi-ellipsoid form. The respiratory minute volume is  $11.34 \text{ l/min}$  for SM and  $9.90 \text{ l/min}$  for TM. Breathing frequency is  $19.9 \text{ min}^{-1}$  and  $15.0 \text{ min}^{-1}$  for SM and TM, respectively. This kind of manikin has been used in many previous studies. A detailed study of the similarities and differences in the breathing dynamics process between these manikins and human subjects has recently been published [53]. For more details concerning the experimental setup and data acquisition see [54].

### 3. Computational model

This section gives details of the numerical model used to accurately predict the cross-infection risk between two people located in a displacement ventilated room as well as all the phenomena involved, such as temperature and velocity gradients or contaminant dispersion.

#### 3.1. Equations

The computational model solves the chemical species, continuity, momentum, energy and turbulence conservation equations given that the problem is three-dimensional, transient and non-isothermal and involves two species. The effect of radiation is included using the surface-to-surface radiation model. The RNGk- $\epsilon$  model that accounts for low-Reynolds-number effects in conjunction with enhanced wall treatment which combines a two-layer model with enhanced wall functions is used in these simulations. The pressure-velocity coupling was resolved using the PISO scheme. A second-order implicit transient formulation is chosen which is unconditionally stable with respect to time-step size. A second-order upwind discretization scheme is used for all equations [55].

#### 3.2. Geometry and grid

The computational geometry replicates in detail the experiments carried out in the full-scale chamber (Fig. 1). Most of the chamber geometry is created with a hexahedron. Only near the manikins and the diffuser has a tetrahedral mesh been used. A conformal mesh joins both blocks of cells. Due to their geometry complexity and the expected high velocity and temperature gradients, mesh refinement was performed around the two manikins, the radiator, the two exhausts, and the diffuser. The mesh is significantly refined at the manikins' faces and in the exhalation zone in order to accurately simulate the interaction between the two breathing flows. Coarse mesh with hexahedral cells was considered for the rest of the room, totaling over one and half million volumes. Details about the manikin geometry and mesh sensitivity study are reported in a previous work [56].

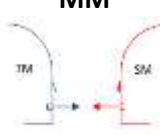
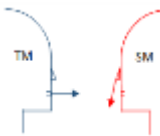
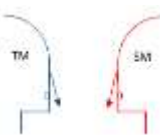
#### 3.3. Boundary and initial conditions

A ventilation flow rate of  $196 \text{ m}^3/\text{h}$  reaches the room at a temperature of  $16.1 \text{ }^\circ\text{C}$  through the wall-mounted semicircular diffuser. The boundary condition for the semicircular diffuser is a uniform velocity of  $0.289 \text{ m/s}$  normal to the curved. A sub-domain with a thickness of  $0.05 \text{ m}$  in front of the semicircular diffuser was defined. A momentum/volume source of  $1.375 \text{ kg s}^{-2} \text{ m}^{-2}$  directed normally to the inlet boundary was given in the sub-domain, generating a radial airflow with constant velocity at the supply covering [57].

The boundary condition for the two exhaust openings is pressure-outlet. The heat power of the radiator is 300 W and the heat load for each manikin is 94 W. The walls of the test chamber are well-insulated and can be considered adiabatic.

The breathing function is a very important point in simulation. The two manikins breathe following a sinusoidal function. There is a half period during which the manikin is exhaling and another half in which the manikin is inhaling. The volume rate is 0.57 l/exhalation for the SM and 0.66 l/exhalation for the TM. Breathing frequency is 20 breaths/minute for the SM and 15 breaths/minute for the TM. The temperature of exhaled air is always 34°C. The mass fraction of N<sub>2</sub>O in the exhaled air of the SM is  $Y_a = 0.027$ . Velocity is normal and uniform in the opening areas: mouth and nostrils. The sizes of the mouth and nostril opening areas differ, such that velocity must be adjusted in order to maintain the same volume rate in exhalation and inhalation. Table 2 shows the velocity boundary conditions of the two manikins.

Table 2. Breathing boundary conditions for the two manikins.  $v > 0$  denotes exhalation and  $v < 0$  denotes inhalation. Mouth area is 122 mm<sup>2</sup> and nostril area is 225 mm<sup>2</sup>.  $A = 2\pi/3$ ,  $B = \pi/2$ . Figures show the exhalation mode of each manikin for the different tests (inhalation was always through the nose).

Test	Target Manikin	Source Manikin
 <p><b>MM</b></p>	$v_{mouth} = \begin{cases} 4.210 \sin Bt & \text{if } v > 0 \\ 0 & \text{if } v < 0 \end{cases}$ $v_{nostril} = \begin{cases} 0 & \text{if } v > 0 \\ 2.293 \sin Bt & \text{if } v < 0 \end{cases}$	$v_{mouth} = \begin{cases} 4.840 \sin At & \text{if } v > 0 \\ 0 & \text{if } v < 0 \end{cases}$ $v_{nostril} = \begin{cases} 0 & \text{if } v > 0 \\ 2.636 \sin At & \text{if } v < 0 \end{cases}$
 <p><b>NM</b></p>	<p>Mouth = Wall</p> $v_{nostril} = 2.293 \sin Bt$	$v_{mouth} = \begin{cases} 4.840 \sin At & \text{if } v > 0 \\ 0 & \text{if } v < 0 \end{cases}$ $v_{nostril} = \begin{cases} 0 & \text{if } v > 0 \\ 2.636 \sin At & \text{if } v < 0 \end{cases}$
 <p><b>MN</b></p>	$v_{mouth} = \begin{cases} 4.210 \sin Bt & \text{if } v > 0 \\ 0 & \text{if } v < 0 \end{cases}$ $v_{nostril} = \begin{cases} 0 & \text{if } v > 0 \\ 2.293 \sin Bt & \text{if } v < 0 \end{cases}$	<p>Mouth = Wall</p> $v_{nostril} = 2.636 \sin At$
 <p><b>NN</b></p>	<p>Mouth = Wall</p> $v_{nostril} = 2.293 \sin Bt$	<p>Mouth = Wall</p> $v_{nostril} = 2.636 \sin At$

There are two places in transient simulations and experiments where an error might occur: during start-up and when letting simulations and experiments run sufficient time to achieve characteristic eddy turnover time [58]. In the experiments, at least four hours are needed to stabilize room conditions before measurements are taken. In the computations, the initial conditions for transient simulations are obtained for a steady simulation and the first 30 minutes of the transient simulation are discarded.

Large eddy turnover time is a characteristic timescale for the domain  $l_0/v_0$  where  $l_0$  is the largest scale of the room and  $v_0$  is the characteristic velocity. In the full-scale test chamber,  $l_0 = 4.1$  m, and an estimation of  $v_0$  can be performed by dividing the ventilation flow rate by a half section of the test chamber. Eddy turnover time is thus about five minutes. In order to obtain a suitable temporal average, a total time of 12 minutes is simulated. To capture the effects of the smaller time scales related to the breathing process a time step of 0.025 s is selected.

Over a 12-second period, SM performed four full breaths (exhalation and inhalation) with TM performing three full breaths during the same period. Each 12 seconds, both manikins start a new breathing cycle. During the 12 minutes of simulation, 60 cycles of 12 seconds are simulated for each test. Figure 2 shows the exhalation flows during a 12-second cycle for the two breathing manikins.

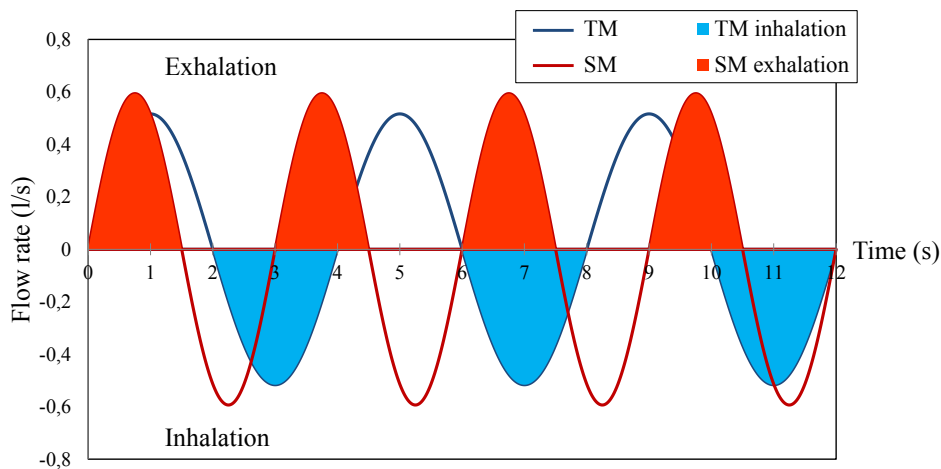


Fig. 2: Instantaneous inhaled and exhaled flow for each manikin in a 12-second cycle. Semi-periods of exhalation of contaminated air by the SM are shaded in red, and the semi-periods of inhalation of contaminated air of the TM are shaded in blue.

## 4. Results and discussion

### 4.1 Experimental validation of the CFD model

Experimental validation of the CFD model using experimental results [52] was performed in two different stages. The purpose of the first stage is to analyze exhalation flow and dispersion of the exhaled contaminants by a single manikin, considered the source manikin (SM), focusing particular attention on the exhalation jet and the interaction with the indoor airflow pattern. For this stage, the experimental setup and corresponding numerical model are exactly the same as described in the previous sections but omitting the TM. Results show a satisfactory agreement of temperature and velocity distribution in the room, airflow pattern from the diffuser, and centerline of the exhalation jet between the numerical simulation and measurements. Detailed information about this process is published in [56].

During the second stage, the TM is added to analyze cross-infection of two people facing each other at different distances in displacement ventilation (DV) conditions. Experimental results [54] with the two manikins exhaling through the mouth and inhaling through the nose and four different distances between the manikins, 0.35, 0.50, 0.80 and 1.10 m, are used to validate the Test MM numerical model. A mixture of air and  $N_2O$  with a mass fraction  $Y_a=0.027$  is exhaled by the SM. Mean  $N_2O$  concentration is measured near

the TM at three different positions (Fig. 3): the chest,  $C_{chest}$ , the nose,  $C_{nose}$ , and 10 cm above the head of the TM,  $C_{10}$ .

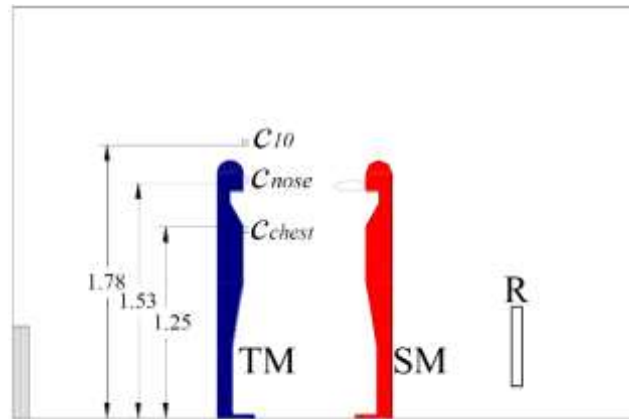


Fig. 3: Sketch of the test room with the manikins and the location of the  $N_2O$  concentration probes at the TM. The separation between manikins in the picture is 0.80 m. All measurements are in meters.

Fig. 4 shows the time averaged experimental and numerical  $N_2O$  concentration values in each location scaling with the mean exhaust concentration of the room  $C_R$ . There is reasonable agreement between numerical and experimental results.

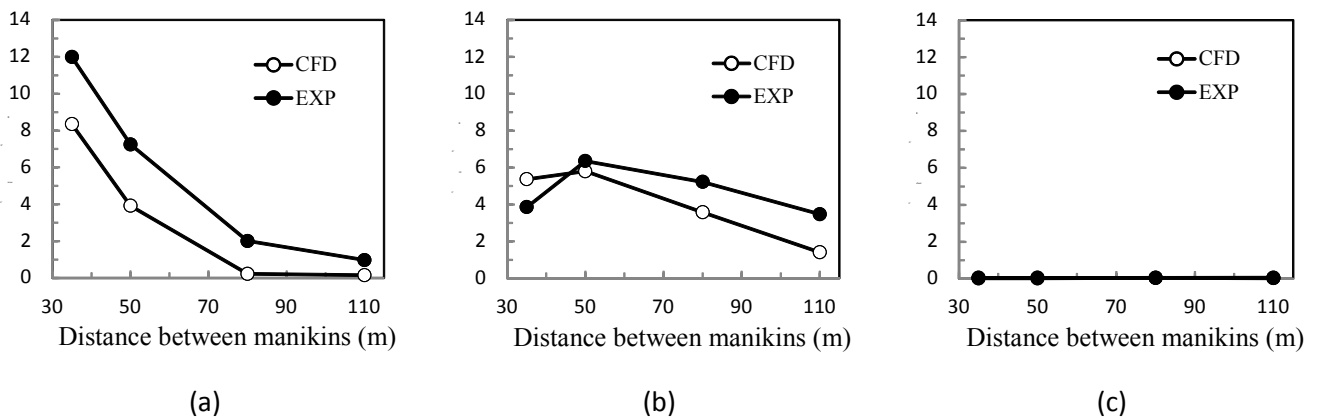


Fig. 4: Mean experimental and numerical dimensionless  $N_2O$  concentration at a)  $C_{nose}$ , b)  $C_{10}$ , c)  $C_{chest}$ . Both manikins breathe out through the mouth, test MM.

The  $N_2O$  concentration in the nose position of the TM, which corresponds to  $C_{nose}$ , (Fig. 4a) decreases with the separation between the manikins. Although the numerical model predicts the same tendency for the four distances, its results show a lower contaminant concentration. The same observation can be found above the head position (Fig. 4b) except for the separation distance of 0.35 m where the numerical prediction is higher than the experimental result. At the height of the chest (Fig. 4c), the contaminant concentration measured and predicted by the numerical model is close to zero due to the thermal stratification of the ventilation strategy that keeps the area below exhalation free of contaminants.

Figure 5 shows the contours of the average  $N_2O$  concentration scaled with the  $N_2O$  concentration exhaled by the SM,  $Y_{or}$ , in the middle plane of the room. For short distances between manikins (0.35 and 0.50 m), exhalation through the mouth of the SM directly penetrates the breathing area of the TM, increasing the contaminant concentration significantly (Fig. 5a and Fig. 5b, respectively). For a separation distance of 0.35 m there is a strong interaction between the two exhalation jets, which have a high momentum, and

thermal plumes leading to a high turbulence level in front of the TM's face. However, for longer distances (0.8 and 1.1 m), exhalation has greater difficulty penetrating the TM's microenvironment (Fig. 5c and Fig. 5d). TM exhalation through the mouth interacts with the exhaled contaminants and pushes them backward, keeping the inhalation region free of contaminants. Moreover, the thermal plume of the TM influences the contaminant distribution making them rise to the upper part of the room and increasing the contaminant concentration in  $C_{10}$ . (See also Fig. 4b and Fig. 4c.).

The results shown here correspond to mean values although the process is highly transient such that previous comments should be tempered by taking into account the analysis of transient data.

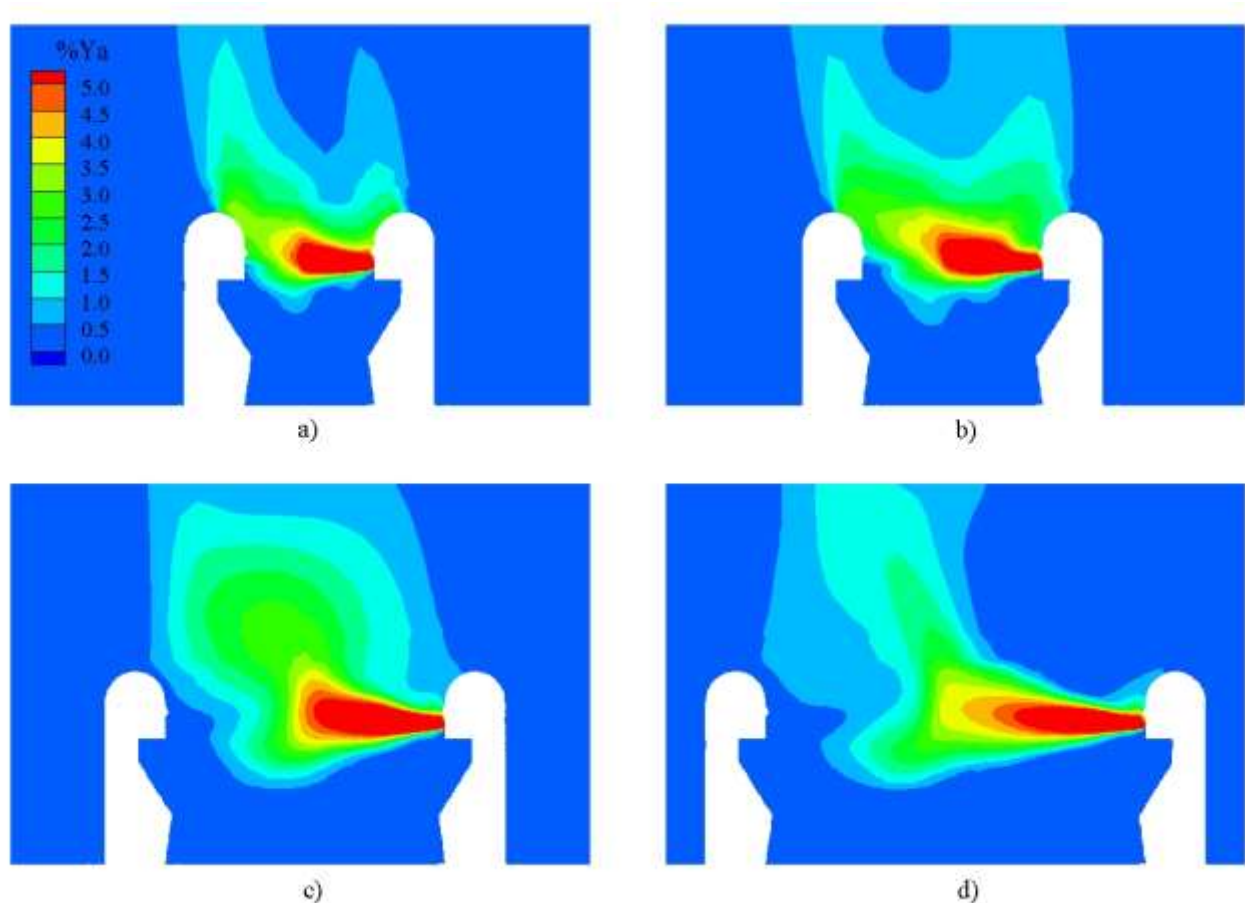


Fig. 5: Mean concentrations of  $N_2O$  in the central plane for the four distances. Test MM. a)  $d=0.35$  m; b)  $d=0.50$  m; c)  $d=0.80$  m and d)  $d=1.10$  m

#### 4.2 Transient analysis

The experimental data do not allow any detailed temporal evolution of the breathing since it is too fast a process for the spectroscopy photoacoustic experimental technique. In this section, the evolution in time of the exhalation process of the two manikins considering different exhalation modes and different distances between them is analyzed. The predicted amount of inhaled contaminant by TM is evaluated.

First, Fig. 6 shows the numerical results of the mass fraction of  $N_2O$  inhaled by the TM during test MM over 12-second cycles. It is important to remember that the two manikins, TM and SM, perform three and four complete breaths, respectively, during that time (see Fig. 2). The phase-averaged method was used to show

these results. The solid line represents the phase-average values and vertical bars represent the minimum and maximum values for 60 cycles.

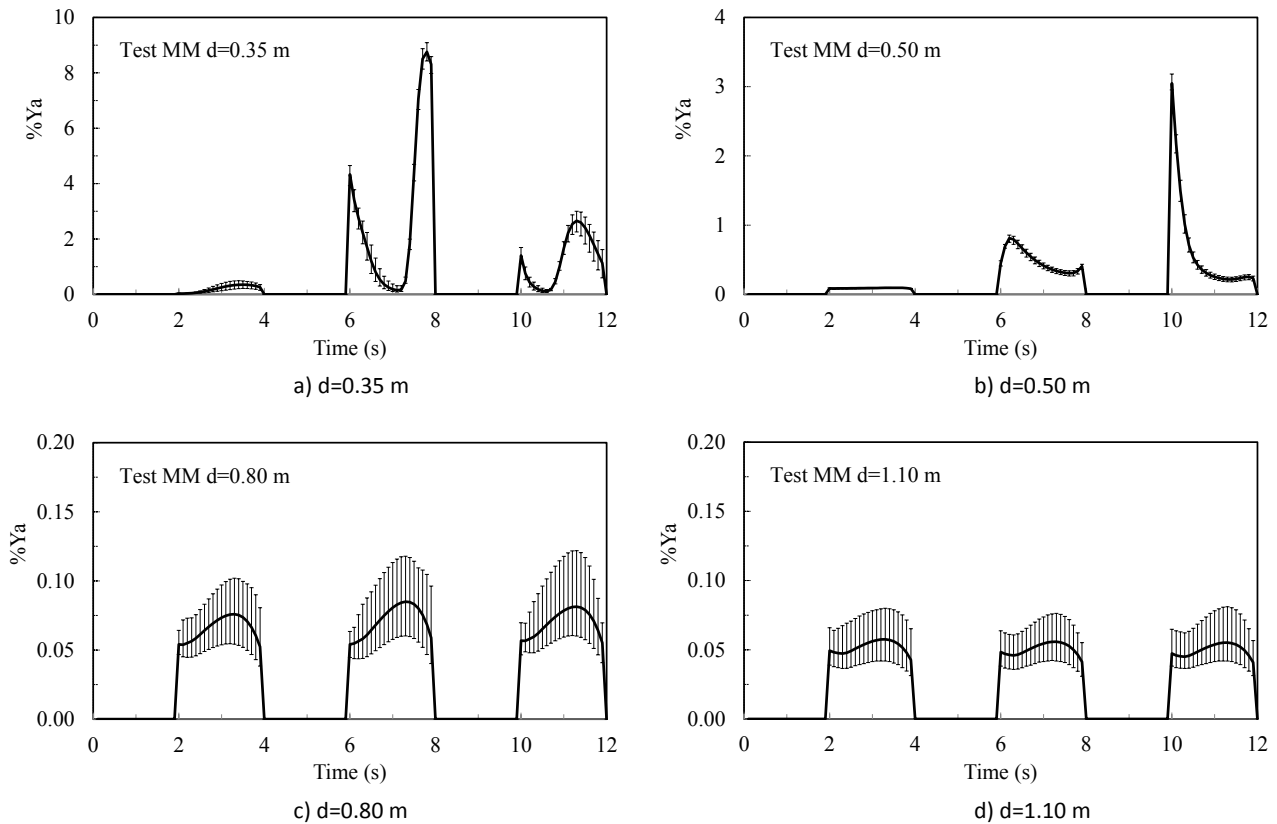


Fig. 6: Concentration of  $N_2O$  inhaled by the TM during 12 sec cycles. N.B. the differences of scales.

When the distance between the manikins is 0.35 m to 0.50 m (Fig. 6a) and Fig. 6b, respectively) the pattern of inhaled contaminants is repeated with great accuracy each 12 s (little cyclical dispersion) as evidenced by the relatively small size of the bars. Moreover, the concentration of contaminants inhaled during the two seconds of each inhalation varies enormously, particularly in the second and third inhalation. Moreover, the maximum inhaled concentration peak is found at different time points. For a separation distance of 0.35 m, it is found at 7.5 seconds from the beginning of the cycle but for a 0.50 m separation distance this peak is found at 10 seconds. The separation distance influences the time in which the SM exhalation reaches the TM breathing area. While for 0.35 m the exhalation from the SM reaches the inhalation area of the TM in 1.4 seconds if there is no perturbation by the TM's exhalation, for 0.50 m this exhalation takes 1.7 seconds to reach the TM. From the above discussion, the significant role played by the breathing frequency and the phase difference between breaths on the amount of  $N_2O$  inhaled is clear, at least when the TM exhales through the mouth and the separation distance is 0.50 m or less.

For  $d=0.80$  m (Fig. 6c) or  $d=1.10$  m (Fig. 6d), the concentration during each inhalation is more even and the cyclical dispersion is notable. This behavior can be observed in the four tests when there is a large separation between manikins ( $d=0.80$  m y  $d=1.10$  m). This is most likely due to the non-stationary nature of the airflow pattern in the area between the two manikins in particular and to the room as a whole. The non-stationary behavior of the general flow in the room can clearly be seen through the changes in the thermal plumes on the heat sources (manikins and radiator) and concurs with previous observations [56].

Secondly, the rate of contaminant that the TM inhales in each of the three inhalations it makes during all the 12 s cycles is shown in Fig. 7. This figure shows the rate of N<sub>2</sub>O inhaled by the TM for the four tests simulated and for the four separation distances. For Test MM and d=0.35 m, 6% of the total amount of N<sub>2</sub>O inhaled is inhaled in the first inhalations, 54% in the second inhalations and 40% in the third inhalations of each 12-second cycle (Fig. 7a). For d=0.50 m, the results are similar. This less noticeable variability is also seen for the case in which the SM exhales through the mouth (test NM) at short distances (d=0.35 m and d=0.50 m) and for test MN when d=0.35 m. In the remaining cases, the proportion of contaminant inhaled in each of the three inhalations is virtually the same.

It could be concluded that when the SM exhales through the mouth and there is a short distance to the TM ( $d \leq 0.50$  m), contamination from the TM depends on the frequencies and respiratory phase differences between the two manikins. In the remaining cases, with the sole exception of test MN for d=0.35 m, the frequencies and respiratory phase differences between the two manikins barely affect the TM contamination.

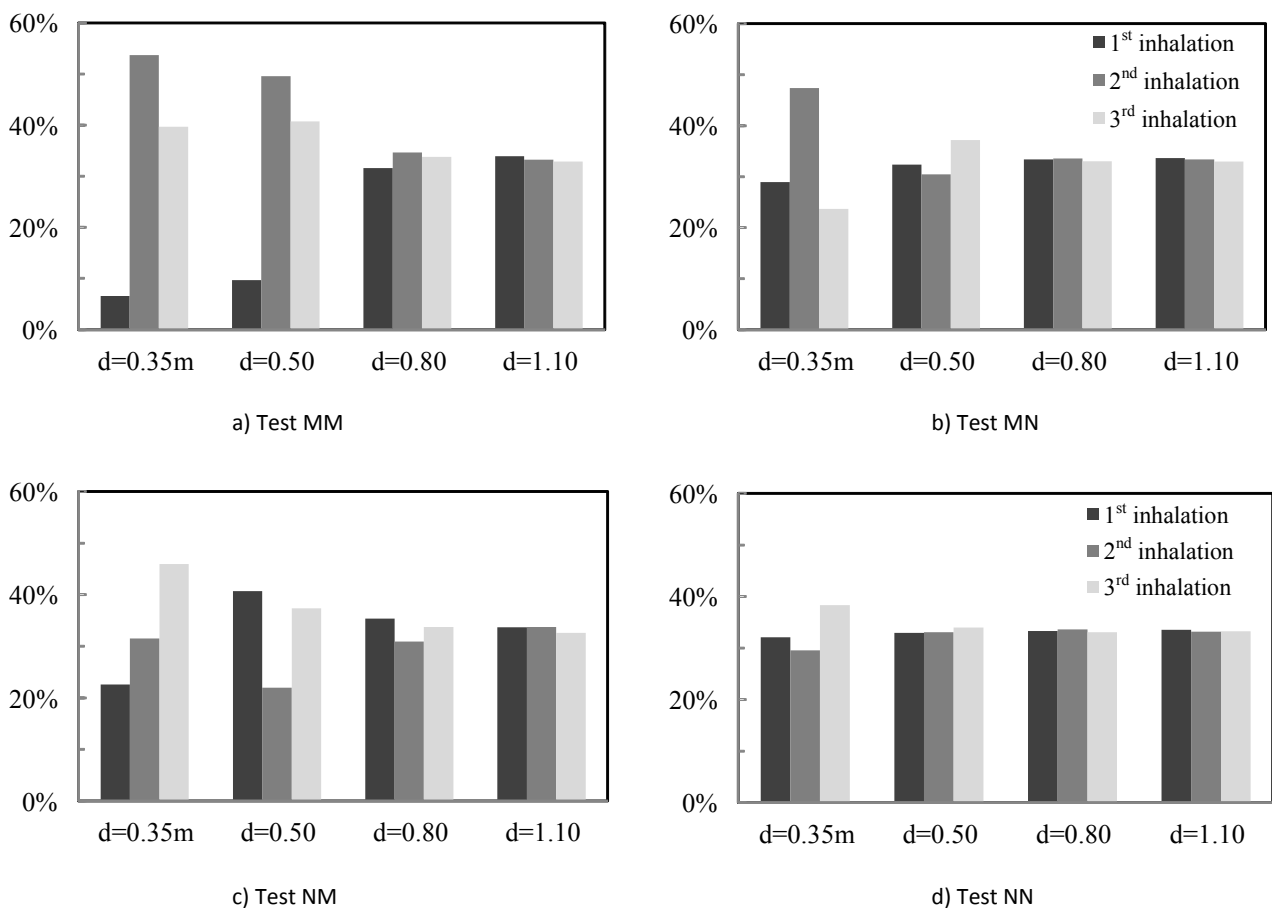


Fig. 7: Percentage of N<sub>2</sub>O inhaled in each of the three inhalations of the 12 s cycle.

Finally, in order to evaluate and increase knowledge of the dispersion of exhaled contaminants and the interaction between the two breaths, Fig. 8 analyzes the temporal evolution of the N<sub>2</sub>O inhaled by the TM for the four tests studied at a separation distance of 0.50 m. As seen in the previous sections, a separation distance of 0.50 m is sufficient to observe the development of the SM exhalation jet and the interaction with the TM's breathing. The isoconcentration values of N<sub>2</sub>O are also shown in Fig. 9 for all the tests at the same

separation distance, 0.5 m for the two first seconds of the cycle. The video shows the results equivalent to those of Fig. 9 for a full 12-second cycle.

Comparing the tests corresponding to SM exhalation through the mouth, Figures 8a and 8b, to the tests where SM exhales through the nose, Figures 8c and 8d, significant differences can be seen. When the SM exhales through the mouth, the TM's three inhalations differ enormously but are repeated with small variations each 12 seconds. Nevertheless, when the SM exhales through the nose, the three inhalations are very similar, yet there is little repetition each 12 seconds. Furthermore, the MM and NM tests show there are higher maximum mass fraction values of inhaled N<sub>2</sub>O but that maximums vary over time depending on the breathing interaction.

The MM test shows the greatest variations (Fig. 8a). During the first instants of each 12-second cycle, the first TM exhalation jet pushes back the first contaminated exhalation from SM, keeping the inhalation area clean during the first inhalation (Fig. 9a). However, 10 s after the beginning of the cycle the SM exhalation jet has reached the TM when the TM is starting to inhale. In that case, there is a maximum peak of inhaled contaminant by the TM.

For the NM test, the risk situation is maintained over time (Fig. 8b) since TM exhalation through the nose disturbs the SM exhalation that can directly penetrate the TM's breathing area (Fig. 9b) very little. However, for the MN and NN tests, when the SM exhales through the nose the maximum values of inhaled contaminant are lower but are almost the same values, and are repeated over time. This means that the direct influence of the SM exhalation jet over the breathing area of the TM is lower (Fig. 9c and Fig. 9d).

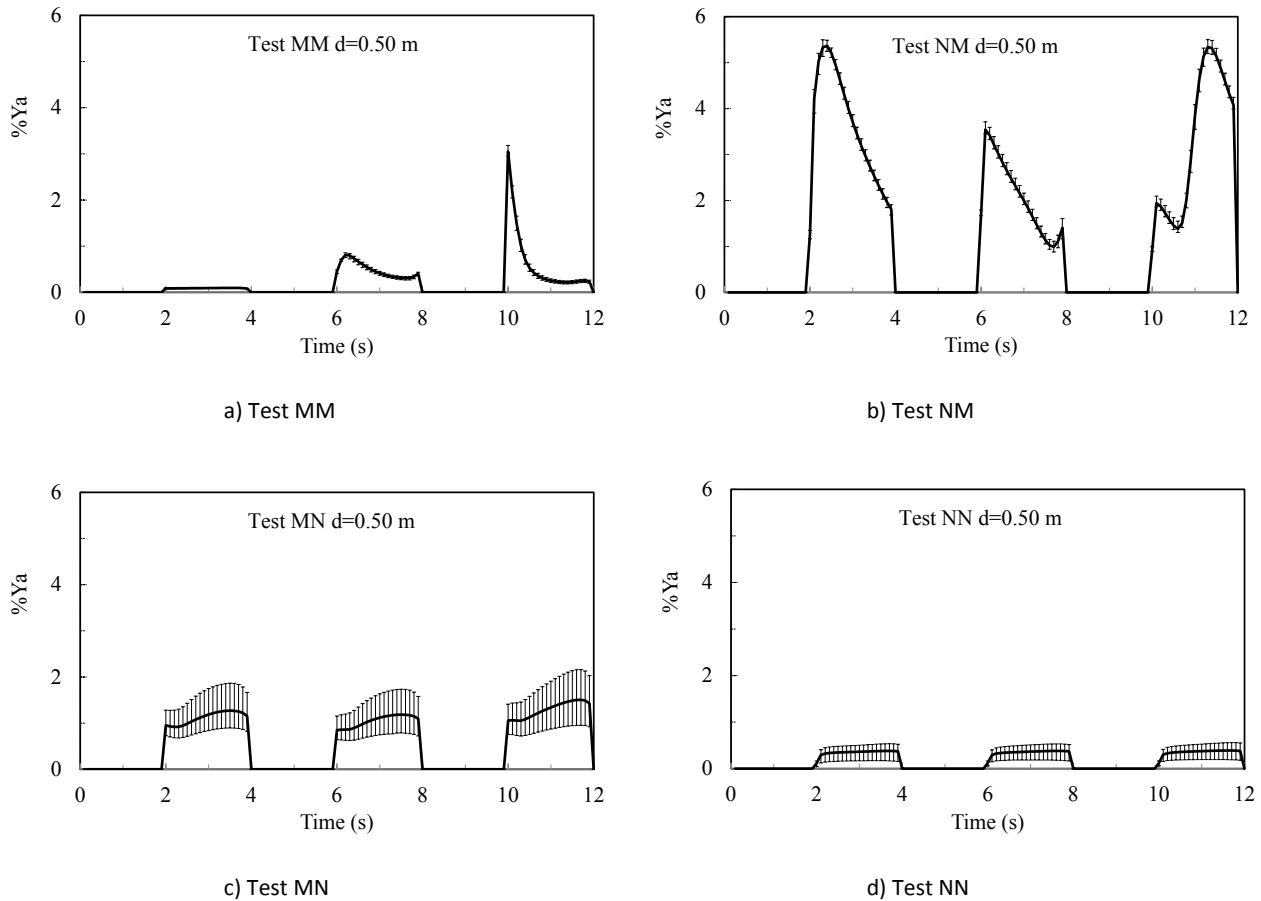


Fig. 8: Concentration of  $N_2O$  inhaled by the TM during 12-second cycles for all breathing modes and  $d=0.50$  m.

When the SM exhales through the nose, tests MN and NN, the exhaled flow of contaminants becomes more complicated (Fig. 9c and Fig. 9d). The flow characteristics are different for the interaction of the two jets. The jet exhaled by the nose first heads downwards and then, as it loses its initial momentum, is dragged upwards by buoyancy. When the TM exhales through the mouth there is scarcely any interference between the exhalations of the two manikins (see  $t=1.0$  s and  $t=1.5$  s of Fig. 9c), and the dispersed jet of the SM's previous exhalation reaches the TM when it is starting the first inhalation ( $t=2.0$  s of Fig. 8c and Fig. 9c). When the two manikins exhale through the nose, their jets interact, favoring dilution of the  $N_2O$  (see  $t=1.0$  s and  $t=1.5$  s of Fig. 9d) such that when the TM commences the first inhalation ( $t=2.0$  s of Fig. 9d) the air close to its nose has a low concentration of  $N_2O$  (Fig. 8d). As there is no direct influence of the SM's exhalation on the breathing area of the TM, the values of inhaled contaminant are more stable over time (Figures 8c and 8d).

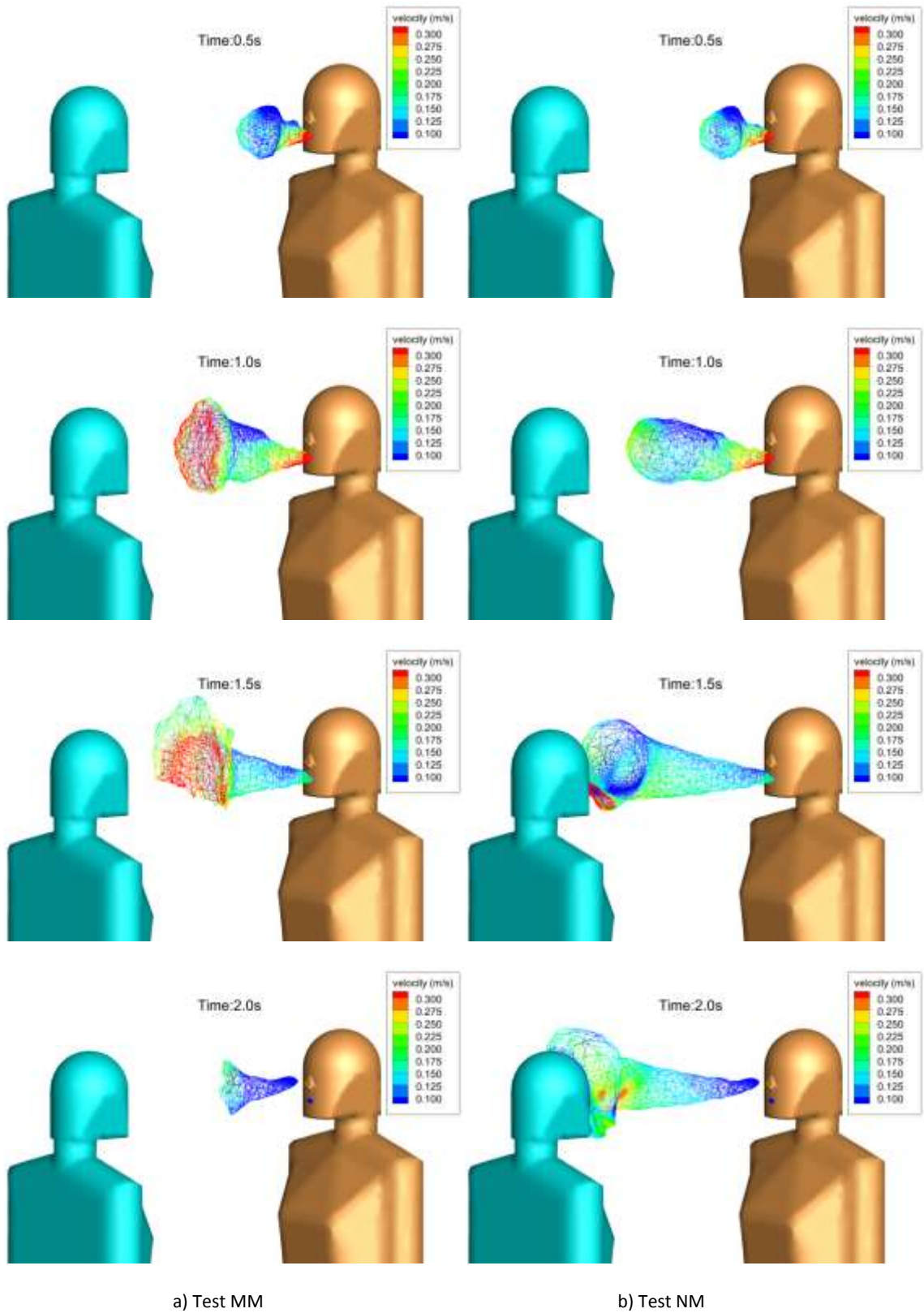


Fig. 9: Isoconcentration environments  $Y=0.05 Y_a$ , shaded in velocity module for a separation between manikins of  $d=50$  cm. The times indicated in each figure correspond to those of Fig. 2.

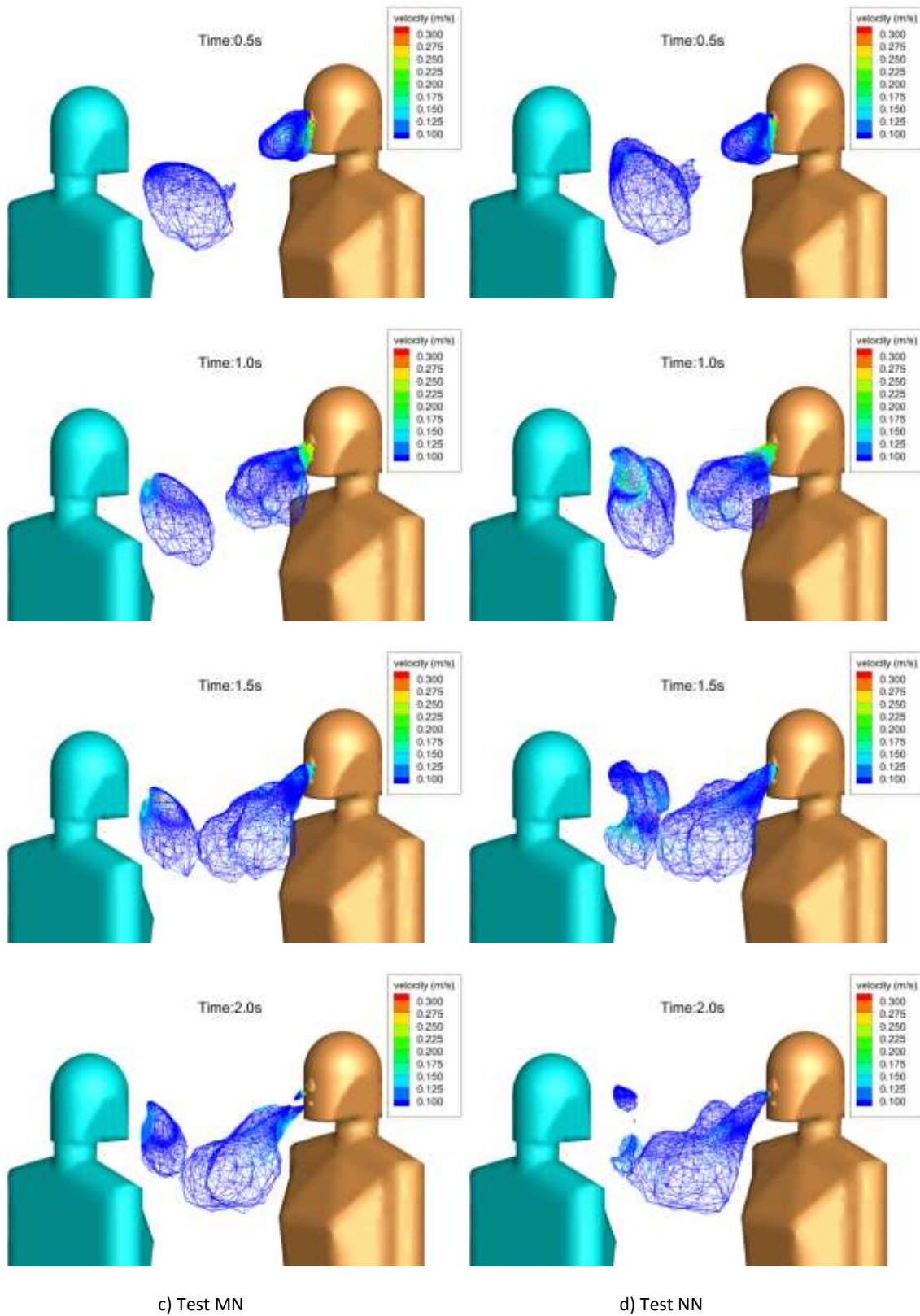


Fig. 9 (cont.) Isoconcentration environments  $Y=0.05Y_a$ , shaded with velocity module for Test MN and Test NN with a separation between manikins of  $d=50$  cm. The times indicated in each figure correspond to those of Fig. 2.

### 4.3 CFD predictions of the risk of cross infection

If the SM represents a person infected with an airborne transmission disease and N<sub>2</sub>O represents pathogen-bearing droplet nuclei, the risk of infection for another person located in the same area (not taking into account the susceptibility of contracting the disease) will be proportional to the amount of N<sub>2</sub>O inhaled by the TM. Nevertheless, the quantity of pathogens exhaled by a person infected in each breath depends on a number of variables. The parameter used to quantify the risk of infection should be independent from the amount of pathogens exhaled. Normalized infection time  $t_{in}$  is defined as the time required for the TM to inhale the same amount of N<sub>2</sub>O as is given off by the SM in a breath. The numerical results give the amount mass of N<sub>2</sub>O inhaled by the TM during the 12 minutes (720 seconds) simulated. Bearing in mind the mass of N<sub>2</sub>O exhaled by the SM in one exhalation it is easy to determine  $t_{in}$ . In this case the following expression is used to calculate the values of Fig. 10.

$$t_{in} = \frac{720 \text{ seconds} \times (\text{mass of N}_2\text{O exhaled by the SM in one exhalation})}{\text{mass of N}_2\text{O inhaled in 720 seconds}}$$

The normalized infection time is related to the concepts of quantum of infection [60] and airborne infection risk [59]. If, for instance, the SM exhaled a quantum in each breath,  $t_{in}$  would be the time required for the TM to have a 63.2% chance of infection [30].

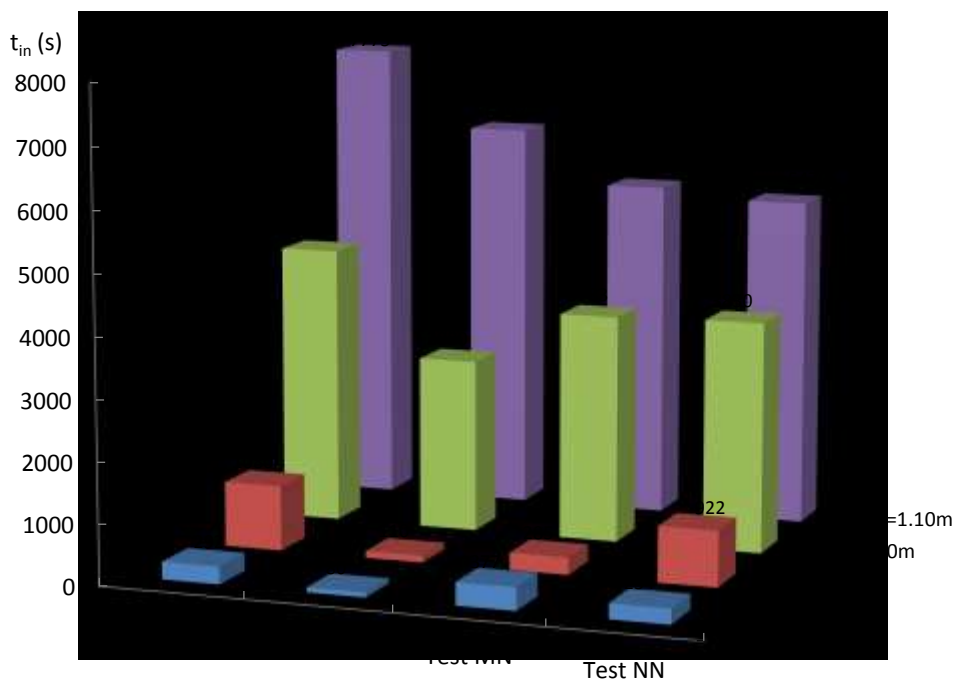


Fig. 10: Infection time for the four breathing modes and the four manikin separation distances.

Figure 10 shows that, regardless of the breathing modes, infection time increases with separation distance. At almost all distances, the lowest infection time is for test NM, when the TM exhales through the nose and the SM exhales through the mouth. This result agrees with the previous analysis of maximum peaks of inhaled contaminants found for that test and continuously over time, Figure 8b. However, the highest infection time is found for test MM, when both manikins exhale through the mouth. It is very interesting to

remember that this test has high peak values of inhaled contaminant but also instances where contaminant inhalation was almost zero. This fluctuating behavior is due to a phase difference between breaths.

## 5. Discussion

The present study provides a numerical analysis of airborne contamination between two manikins facing each other in a room with displacement ventilation. The transient numerical models reproduce the experimental setup in detail [54]. Agreement between the numerical predictions obtained during test MM (see Fig. 4) shows that the numerical model is able to predict the dispersion of exhaled contaminants with a satisfactory accuracy.

Four breathing modes and four separation distances between manikins are analyzed. Sixteen cases are thus studied in a four by four matrix. The results of CFD predictions are an extremely valuable tool for studying, analyzing and gaining insights into the mechanisms of airborne transmission routes. Of particular interest is the analysis of the contaminant dispersion over time, for different separation distances and when they have different breathing modes.

A priori, the riskiest exhalation mode of SM is from the mouth because contaminants are able to penetrate the TM's breathing region very directly, especially if the two manikins are close to each other (see Fig. 9). However, the penetration of the contaminants exhaled by SM in the TM's breathing area also depends on the TM's breathing mode. Exhalation through the TM's mouth can clean the TM's breathing area of contaminants, while exhalation through the TM's nose is not able to remove contaminants from the breathing area. This marks a clear difference between the two cases, with the MM test being the one with the highest infection time and the NM test the one with the lowest infection time (see Fig. 10).

When the SM exhales through the nose it is difficult for the exhalation jet to penetrate into the breathing area of the TM even when the manikins are close to each other. The downward direction of exhalation through the nose leads to the contaminants mixing with the room air before ascending due to buoyancy and reaching the breathing area of the TM if the manikins are close to each other (see Fig. 9). This means that the inhaled contaminants for tests MN and NN are very constant over time and do not show very high peak values (see Fig. 8). Generally speaking, the exhaled contaminants are more likely to reach the breathing area of the TM more diluted when SM exhales through the nose.

When there is a short distance between manikins and, more importantly, if the SM also exhales through the mouth (see blue cases in Table 3), the amount of contaminant inhaled by the TM is strongly determined by the mutual interaction between the breaths of the two manikins but is barely influenced by the general flow pattern in the room. Both circumstances should be taken into account when planning experimental and numerical assays. The time required to simulate numerically and the measuring time in the experimental assays is considerably reduced. However, the time-step of the numerical simulations and the response in frequency of the experimental techniques should be able to reflect the transitory nature of the respiratory cycles.

In contrast, when the manikins are further apart or when the TM exhales through the nose (see green cases in Table 3), the flow pattern in the room has a greater influence on cross-infection than the manikins' frequencies and respiratory phase differences. Similar to what was mentioned in the previous paragraph, in order to obtain reliable statistical averages long simulation and sampling times are required although acquisition frequency and time-step do not need to be very demanding.

Table 3: Summary. Dark blue (DB): cases where the predominant effect is the interaction between both breaths. Dark green (DG): cases where the predominant effect is the general air flow pattern of the room. Light colors (LB, LG): similar to the corresponding dark color but less pronounced behavior.

Test	Distance between manikins			
	0.35 m	0.50 m	0.80 m	1.10 m
MM	DB	DB	LG	DG
NM	DB	DB	LG	DG
MN	DB	LB	DG	DG
NN	LB	DG	DG	DG

Finally, it is also important to show that a certain breathing mode combination of the two manikins can evidence very high values of inhaled contaminants at specific instances but a low value of cross-infection risk during a global period of time, for example test MM. This analysis is only possible by means of CFD due to the low frequency of the experimental contaminant concentration measurements.

## Conclusions

In this study, the full interaction between two breaths is studied by means of CFD and shows accurate results. The main conclusion of this research is to evidence the high capacity of numerical simulations to analyze the dispersion of exhaled contaminants over time, including interaction with other breathing sources and in different situations. At look at the results provides certain key conclusions in the study of airborne risk situations in indoor environments:

- The different modes a person may use for breathing can directly influence the microenvironment around them as well as the interaction with another person's breathing. This means that exhaling through the mouth or through the nose may disperse exhaled contaminants in a completely different way and may also prevent exhaled contaminants from being received differently.
- The aerodynamic information obtained with CFD complements experimental measurements and increases knowledge of the mechanism involved in the airborne transmission route of contaminants.
- For short separation distances (<0.5 m) between breathing sources, the microenvironment and the interaction between breaths is a key factor in the dispersion of contaminants for all the breathing mode combinations studied. However, for long distances (>0.5 m) the interaction between breaths, for example if they are in phase or not, is not an important issue. For these cases, the general airflow conditions in the room or the macroenvironment prove to be more important.

## Acknowledgment

This research was supported by projects DPI2014-55357-C2-1-R and DPI2014-55357-C2-2-R from the Spanish National Government 2013-2016 R&D&I plan issued by the Ministry of Economy and Competiveness.

## References

[1] Nielsen PV. Flow in air conditioned rooms: Model experiments and numerical solution of the flow equations. 1974.

[2] Awbi HB. Application of computational fluid dynamics in room ventilation. Build Environ 1989;24:73-84.

- [3] Gan G. Evaluation of room air distribution systems using computational fluid dynamics. *Energy Build* 1995;23:83-93.
- [4] Chen Q. Prediction of room air motion by Reynolds-stress models. *Build Environ* 1996;31:233-44.
- [5] Nielsen PV. Description of supply openings in numerical models for room air distribution. *ASHRAE Transactions* 1992;98:963-70.
- [6] Posner JD, Buchanan CR, Dunn-Rankin D. Measurement and prediction of indoor air flow in a model room. *Energy Build* 2003;35:515-26.
- [7] Fontaine JR, Rapp R, Koskela H, Niemelä R. Evaluation of air diffuser flow modelling methods experiments and computational fluid dynamics simulations. *Build Environ* 2005;40:377-89.
- [8] Huo Y, Haghghat F, Zhang JS, Shaw CY. A systematic approach to describe the air terminal device in CFD simulation for room air distribution analysis. *Build Environ* 2000;35:563-76.
- [9] Srebric J, Chen Q. Simplified numerical models for complex air supply diffusers. *HVAC&R* 2002:277-94.
- [10] Wan MP, Chao CY. Numerical and experimental study of velocity and temperature characteristics in a ventilated enclosure with underfloor ventilation systems. *Indoor Air* 2005;15:342-55.
- [11] Kim T, Kato S, Murakami S, Rho J-. Study on indoor thermal environment of office space controlled by cooling panel system using field measurement and the numerical simulation. *Build Environ* 2005;40:301-10.
- [12] He G, Yang X, Srebric J. Removal of contaminants released from room surfaces by displacement and mixing ventilation: Modeling and validation. *Indoor Air* 2005;15:367-80.
- [13] Richmond-Bryant J, Eisner AD, Brixey LA, Wiener RW. Transport of airborne particles within a room. *Indoor Air* 2006;16:48-55.
- [14] Lee E, Khan JA, Feigley CE, Ahmed MR, Hussey JR. An investigation of air inlet types in mixing ventilation. *Build Environ* 2007;42:1089-98.
- [15] Srebric J, Vukovic V, He G, Yang X. CFD boundary conditions for contaminant dispersion, heat transfer and airflow simulations around human occupants in indoor environments. *Build Environ* 2008;43:294-303.
- [16] Corgnati SP, Perino M, Fracastoro GV, Nielsen PV. Experimental and numerical analysis of air and radiant cooling systems in offices. *Build Environ* 2009;44:801-6.
- [17] Halvonová B, Melikov AK. Performance of "ductless" personalized ventilation in conjunction with displacement ventilation: Impact of disturbances due to walking person(s). *Build Environ* 2010;45:427-36.
- [18] Tian ZF, Tu JY, Yeoh GH, Yuen RKK. On the numerical study of contaminant particle concentration in indoor airflow. *Build Environ* 2006;41:1504-14.
- [19] Tang JW, Noakes CJ, Nielsen PV, Eames I, Nicolle A, Li Y et al. Observing and quantifying airflows in the infection control of aerosol- and airborne-transmitted diseases: an overview of approaches. *J Hosp Infect* 2011;77:213-22.

- [20] Wurie FB, Lawn SD, Booth H, Sonnenberg P, Hayward AC. Bioaerosol production by patients with tuberculosis during normal tidal breathing: Implications for transmission risk. *Thorax* 2016;71:549-54.
- [21] King M-, Noakes CJ, Sleigh PA, Camargo-Valero MA. Bioaerosol deposition in single and two-bed hospital rooms: A numerical and experimental study. *Build Environ* 2013;59:436-47.
- [22] Qian H, Li Y, Nielsen PV, Huang X. Spatial distribution of infection risk of SARS transmission in a hospital ward. *Build Environ* 2009;44:1651-8.
- [23] Yu ITS, Li Y, Wong TW, Tam W, Chan AT, Lee JHW et al. Evidence of Airborne Transmission of the Severe Acute Respiratory Syndrome Virus. *N Engl J Med* 2004;350:1731-9.
- [24] Yam R, Yuen PL, Yung R, Choy T. Rethinking hospital general ward ventilation design using computational fluid dynamics. *J Hosp Infect* 2011;77:31-6.
- [25] Li Y, Huang X, Yu ITS, Wong TW, Qian H. Role of air distribution in SARS transmission during the largest nosocomial outbreak in Hong Kong. *Indoor Air* 2004;15:83-95.
- [26] Liu J, Wang H, Wen W. Numerical simulation on a horizontal airflow for airborne particles control in hospital operating room. *Build Environ* 2009;44:2284-9.
- [27] Chow TT, Yang XY. Performance of ventilation system in a non-standard operating room. *Build Environ* 2003;38:1401-11.
- [28] Qian H, Li Y. Removal of exhaled particles by ventilation and deposition in a multibed airborne infection isolation room. *Indoor Air* 2010;20:284-97.
- [29] Cheong KWD, Phua SY. Development of ventilation design strategy for effective removal of pollutant in the isolation room of a hospital. *Build Environ* 2006;41:1161-70.
- [30] Villafruela JM, Castro F, José JFS, Saint-Martin J. Comparison of air change efficiency, contaminant removal effectiveness and infection risk as IAQ indices in isolation rooms. *Energy Build* 2013;57:210-9.
- [31] Yang C, Yang X, Zhao B. The ventilation needed to control thermal plume and particle dispersion from manikins in a unidirectional ventilated protective isolation room. *Building Simulation* 2015:1-15.
- [32] Hathway EA, Noakes CJ, Sleigh PA, Fletcher LA. CFD simulation of airborne pathogen transport due to human activities. *Build Environ* 2011;46:2500-11.
- [33] King M-, Noakes CJ, Sleigh PA. Modeling environmental contamination in hospital single- and four-bed rooms. *Indoor Air* 2015;25:694-707.
- [34] Lin Z, Wang J, Yao T, Chow TT. Investigation into anti-airborne infection performance of stratum ventilation. *Build Environ* 2012;54:29-38.
- [35] He Q, Niu Ji, Gao N, Zhu T, Wu J. CFD study of exhaled droplet transmission between occupants under different ventilation strategies in a typical office room. *Build Environ* 2011;46:397-408.
- [36] Fišer J, Jícha M. Impact of air distribution system on quality of ventilation in small aircraft cabin. *Build Environ* 2013;69:171-82.

- [37] Chen C, Lin CH, Long Z, Chen Q. Predicting transient particle transport in enclosed environments with the combined computational fluid dynamics and Markov chain method. *Indoor Air* 2014;24:81-92.
- [38] Zhang L, Li Y. Dispersion of coughed droplets in a fully-occupied high-speed rail cabin. *Build Environ* 2012;47:58-66.
- [39] Gao N, Niu Ji. Transient CFD simulation of the respiration process and inter-person exposure assessment. *Build Environ* 2006;41:1214-22.
- [40] Yin Y, Gupta JK, Zhang X, Liu J, Chen Q. Distributions of respiratory contaminants from a patient with different postures and exhaling modes in a single-bed inpatient room. *Build Environ* 2011;46:75-81.
- [41] Chen C, Lin C-, Jiang Z, Chen Q. Simplified models for exhaled airflow from a cough with the mouth covered. *Indoor Air* 2014;24:580-91.
- [42] Seepana S, Lai ACK. Experimental and Numerical Investigation of Interpersonal Exposure of Sneezing in a Full-Scale Chamber. *Aerosol Sci Technol* 2012;46:485-93.
- [43] Tang JW, Nicolle AD, Klettner CA, Pantelic J, Wang L, Suhaimi AB et al. Airflow Dynamics of Human Jets: Sneezing and Breathing - Potential Sources of Infectious Aerosols. *PLoS ONE* 2013;8.
- [44] Li X, Inthavong K, Tu J. Particle inhalation and deposition in a human nasal cavity from the external surrounding environment. *Build Environ* 2012;47:32-9.
- [45] Zhu S, Kato S, Murakami S, Hayashi T. Study on inhalation region by means of CFD analysis and experiment. *Build Environ* 2005;40:1329-36.
- [46] Naseri A, Abouali O, Ghalati PF, Ahmadi G. Numerical investigation of regional particle deposition in the upper airway of a standing male mannequin in calm air surroundings. *Comput Biol Med* 2014;52:73-81.
- [47] Hayashi T, Ishizu Y, Kato S, Murakami S. CFD analysis on characteristics of contaminated indoor air ventilation and its application in the evaluation of the effects of contaminant inhalation by a human occupant. *Build Environ* 2002;37:219-30.
- [48] Habchi C, Ghali K, Ghaddar N, Shihadeh A. Chair fan-enhanced displacement ventilation for high IAQ: Effects on particle inhalation and stratification height. *Build Environ* 2015;84:68-79.
- [49] Feng L, Yao S, Sun H, Jiang N, Liu J. TR-PIV measurement of exhaled flow using a breathing thermal manikin. *Build Environ* 2015;94:683-93.
- [50] Xu C-, Gong G-, Wang Y-, Nielsen PV, Liu L. Effect of air stability on the continuous and periodic exhalation flow of a person. *Hunan Daxue Xuebao* 2014;41:106-12.
- [51] Xu C, Nielsen PV, Gong G, Jensen RL, Liu L. Influence of air stability and metabolic rate on exhaled flow. *Indoor Air* 2015:198-200.
- [52] Olmedo I, Nielsen PV, Ruiz de Adana M, Jensen RL, Grzelecki P. Distribution of exhaled contaminants and personal exposure in a room using three different air distribution strategies. *Indoor Air* 2012;22:64-76.
- [53] Xu C, Nielsen PV, Gong G, Liu L, Jensen RL. Measuring the exhaled breath of a manikin and human subjects. *Indoor Air* 2015:188-197.

[54] Olmedo I. Indoor airflow patterns, dispersion of human exhalation flow and risk of airborne cross-infection between people in a room. Universidad de Córdoba, Servicio de Publicaciones 2012.

[55] FLUENT. Fluent 12.0 user's guide. Lebanon, NH: Fluent Inc., 2009.

[56] Villafruela JM, Olmedo I, Ruiz de Adana M, Méndez C, Nielsen PV. CFD analysis of the human exhalation flow using different boundary conditions and ventilation strategies. *Build Environ* 2013;62:191-200.

[57] Einberg G, Hagström K, Mustakallio P, Koskela H, Holmberg S. CFD modelling of an industrial air diffuser—predicting velocity and temperature in the near zone. *Build Environ* 2005;40:601-15.

[58] Knight KJ, Debus KK. Practical application of the LES method to mixing in large indoor spaces. *Proceedings of IMECE2005* 2005;IMECE2005-82025:587-94.

[59] Riley EC, Murphy G, Riley RL. Airborne spread of measles in a suburban elementary school. *Am J Epidemiol* 1978;107:421-32.

[60] Wells WF. *Airborne Contagion and Air Hygiene. An Ecological Study of Droplet Infections*. Cambridge, MA.: Harvard University Press, 1955.